Nuclear Engineering and Technology 58 (2026) 104203

Contents lists available at ScienceDirect

Nuclear Engineering and Technology

journal homepage: www.elsevier.com/locate/net

Original Article

Optics and beam dynamics study of the ISOLDE superconducting recoil separator

Fazel Taft [a,*], Jorge Giner Navarro [a], Teresa Kurtukian-Nieto [b], Ismael Martel [c], Javier Resta-López [a,d]

[a] Institut de Ciència dels Materials Universitat de València (ICMUV), Carrer del Catedràtic José Beltrán Martinez 2, 46071, Paterna, Spain
[b] Instituto de Estructura de la Materia, CSIC, Calle Serrano 113, 28006, Madrid, Spain
[c] Departamento de Ciencias Integradas, Universidad de Huelva, Avda. Fuerzas Armadas s/n, 21071, Huelva, Spain
[d] Departamento de Electromagnetismo y Física Aplicada, Universitat de València, Carrer del Dr. Moliner 50, 46100, Burjassot, Spain

ARTICLE INFO

Keywords:
Mass spectrometry
Isochronous ring
Superconducting magnets
Time-of-flight

ABSTRACT

The spectrometry of radionuclides is a key area in nuclear physics, driven by the global quest to discover and characterize exotic isotopes. We propose a versatile and compact storage ring, the ISOLDE Superconducting Recoil Separator (ISRS), envisioned as an innovative high-performance spectrometer for HIE-ISOLDE at CERN. The design incorporates ten iron-free superconducting combined-function Canted Cosine-Theta magnets, taking as a reference the so-called MAGDEM prototype, which is also being developed as part of the ISRS project. Using the actual dimensions of MAGDEM, this study explores the beam dynamics possibilities for the ISRS ring, with a particular focus on its performance as a separator for high rigidity beams, up to 2 T m. Taking $^{234}Ra^{+53}$ at 10 MeV/u as the reference ion, the ring operates under isochronous conditions, enabling separation of isotopes based on their mass-to-charge ratios relative to the reference ion. Time-of-Flight (ToF) detection is proposed after only ten turns. Alternative beam dynamics configurations are considered, particularly around the isochronicity condition, which offer greater stability conditions of the circulating beam. These approaches focus on studying key lattice and beam optics parameters, such as momentum acceptance, and ring tune, while also illustrating a practical case of isotope separation.

1. Introduction

The investigation and analysis of nuclear isotopes remain a central focus of scientific inquiry worldwide. Mass spectrometry stands out as a powerful tool for investigating nuclear structures, owing to its exceptional precision in isotope identification [1]. However, the challenge of analyzing short-lived isotopes requires the development of innovative, high-precision mass spectrometry techniques [2]. Traditional linear spectrometers, while effective, require substantial infrastructure and can be costly to operate. Particle storage rings also involve significant investment, but they offer major advantages, most notably, the ability to perform repeated, high-precision measurements on the same ions, greatly enhancing mass accuracy and resolution [3]. Ion trapping provides another storage-based approach; however, its efficiency is limited when dealing with low-energy ion beams [4]. Storage rings, powered by strong electromagnetic fields, provide an advanced and efficient method for confining and detecting particles. In this approach, particles follow circular trajectories, passing through various electric and magnetic fields that influence their orbits. These controlled interactions allow the particles to circulate repeatedly within the ring, significantly enhancing the system's analytical capabilities. As a result, storage rings are valuable tools for high-precision experiments and measurements.

A limited number of facilities worldwide utilize storage rings as spectrometers, yet they enable cutting-edge research across multiple disciplines. However, new methods for particle detection are continuously developed. One of the most widely used technique is the Schottky mass spectrometry (SMS), extensively applied at facilities such as the FRS-ESR at GSI [5,6]. Specifically developed for storage ring environments, SMS offers highly accurate mass measurements. However, the technique presents key limitations: it requires long ion cooling times, making it unsuitable for very short-lived isotopes that may decay before cooling is completed. Additionally, the setup demands significant space to accommodate the cooling infrastructure.

To address such limitations, Isochronous Mass Spectrometry (IMS)

* Corresponding author.
E-mail address: fazel.taft@uv.es (F. Taft).

https://doi.org/10.1016/j.net.2026.104203
Received 4 December 2025; Received in revised form 12 February 2026; Accepted 15 February 2026
Available online 16 February 2026

has emerged as a groundbreaking technique, capable of delivering rapid and precise mass measurements for isotopes with lifetimes as short as a few microseconds. This approach has also been successfully implemented in CSRe storage ring at the Institute of Modern Physics (IMP) in Lanzhou [7], and further advanced through innovations at the RIKEN Rare RI Ring [3].

The IMS approach is now being considered for a new experiment, the ISOLDE Superconducting Recoil Separator (ISRS) [8], which is planned for implementation at the High Intensity and Energy ISOLDE (HIE-ISOLDE) linear accelerator at CERN [9]. This linac is capable of accelerating radioactive isotopes to energies between 0.5 and 10 MeV/u, producing over 1300 isotopes spanning more than 70 elements, from He to Ra. As part of this work, several design configurations have been proposed and developed for the ISRS ring spectrometer to support a range of experimental activities within the ISOLDE program [8,10,11].

The ISRS ring would be a high-precision spectrometer for advanced ion analysis, supporting a wide range of investigations in nuclear physics, astrophysics, and fundamental science. Its ability to store and probe rare isotopes can enable detailed studies of nuclear interactions and structural dynamics. Beyond basic research, ISRS has also the potential to contribute to medical physics through isotope development and ion beam characterization for clinical applications. In principle, with a 5×5 m^2 footprint, the ISRS ring offers a compact solution. For performance evaluation in this work, ^{234}Ra at 10 MeV/u is selected as the reference radionuclide.

The initial proposal [12] introduced a Fixed-Field Alternating Gradient (FFAG) [13,14] design featuring compact 90-degree, strongly curved bending magnets operating in a combined-function mode. In this configuration, a dipolar magnetic field bends the beam trajectory, while an alternating-gradient quadrupole triplet provides transverse focusing/defocusing. The magnet technology adopted for this purpose is based on superconducting Canted Cosine-Theta (CCT) designs, incorporating two inner coils for dipole fields and two nested outer trim coils for quadrupole fields. However, the technical challenges in fabricating such magnets prompted the development of an alternative design: a straight, superconducting CCT magnet that integrates the dipole field and a single quadrupole mode within a unified structure.

We present a new design of the ring that makes use of such magnets, as shown schematically in Fig. 1. The spectrometer operates under isochronous conditions, enabling separation of isotopes based on their mass-to-charge ratios relative to the reference ion and providing high-precision measurements. Time-of-Flight (ToF) detection is inserted after ten turns; however, the system is designed to support extended measurements beyond this baseline, offering flexibility for diverse experimental applications. As alternative beam dynamics, quasi-isochronous configurations are also considered in this article, which offer greater stability conditions of the circulating beam, particularly around the isochronous condition. These approaches focus on studying key lattice and beam optics parameters, such as momentum acceptance, and ring tune, while also illustrating a practical case of heavy-mass ion separation. This analysis provides detailed insights into the performance and capabilities of the ring, paving the way for advanced applications in isotopes separation and relevant studies.

The outline of this article is as follows. Section 2 introduces the operating principle of the isochronous mode in the ISRS spectrometer ring. Section 3 describes the specifications of the CCT magnets that compose the ring. In Section 4, we present the lattice and optical design that enable isochronous operation, along with an alternative quasi-isochronous configuration. Section 5 presents the optical characterization, focusing primarily on the analysis of the beam's betatron tunes, its chromaticity, and their relation to lattice resonances. Section 6 evaluates the ring's performance through tracking simulations, focusing on ToF separation of various radium isotopes with different charge states. Finally, Section 7 discusses the proposed concept and presents the conclusions.

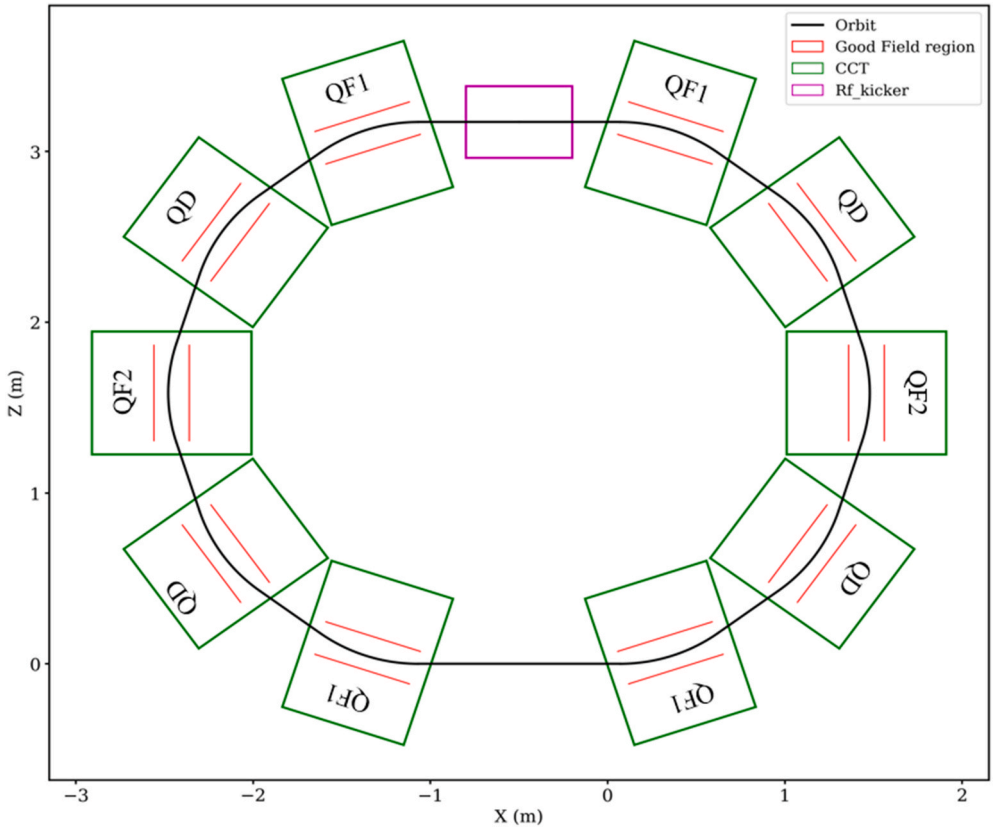

Fig. 1. Schematic of the ring with CCT dimensions. QF: Focusing Gradient, QD: Defocusing Gradient.

2. Principle of the ISRS ring

The principle of the spectrometer ring is based on ToF techniques of particles stored in the ring. Considering an ion with a certain difference in mass-to-charge ratio $\Delta(m/q)$ and a velocity deviation Δv with respect to the reference ion circulating in the storage ring, the revolution period deviation is given by the following expression [15]:

$$\frac{\Delta T}{T} = \frac{1}{\gamma_t^2}\frac{\Delta(m/q)}{m/q} - \left(1 - \frac{\gamma^2}{\gamma_t^2}\right)\frac{\Delta v}{v} + \frac{\Delta T_{HO}}{T}, \quad (1)$$

where γ is the Lorentz factor, and $\gamma_t = 1/\sqrt{\alpha_c}$ is the transition energy factor of the ring, with α_c the momentum compaction factor, which relates the path length deviation from the reference orbit ($\Delta C/C$) with the magnetic rigidity deviation ($\Delta(B\rho)/(B\rho)$):

$$\alpha_c = \frac{1}{\gamma_t^2} = \frac{\Delta C/C}{\Delta(B\rho)/(B\rho)} = \frac{1}{C}\oint \frac{D_x(s)}{\rho} \mathrm{d}s,$$

where C is the length of the reference orbit, $D_x(s)$ the first order dispersion function and ρ the local bending radius.

From Eq. (1), one can see that the second term on the right-hand side depends on the velocity deviation, thus limiting the precise mass measurements.

To ensure a constant revolution time in a storage ring that depends only on the mass-to-charge ratio of the particles, it is essential to eliminate the momentum-dependent variations introduced by the second term in Eq. (1). This can be addressed through two methods. The first is ion cooling [16], where faster ions reduce their velocity when passing through a cooled environment. This process allows all ions in the ring to achieve the same velocity, thereby significantly minimizing velocity spread. so, the term $\Delta v/v$ would approach zero. The second approach is to match the ring to operate in isochronous mode [17,18], where the transition gamma is approximately equal to the Lorentz factor, $\gamma \approx \gamma_t$, so the term known as phase slip factor, η, would approach to zero:

$$\eta = \frac{1}{\gamma^2} - \frac{1}{\gamma_t^2} \approx 0 .$$

At this point, it is necessary to remark that although this isochronous condition is generally valid, the resolution of the measurement of the mass-to-charge ratio also depends on higher-order contributions, which are included in the term $\Delta T_{HO}/T$ of Eq. (1). For instance, higher-order contributions can arise from optical non-linearities and aberrations, magnetic field errors, and fringe-field effects. In future studies, we plan to investigate in detail the performance of the ISRS lattice under the presence of magnetic high-order harmonics and imperfections as well as correction methods to counteract their effects.

In isochronous rings, faster particles, which travel along longer orbits, and slower particles, which follow shorter orbits, naturally adjust their paths to ensure that the revolution time depends solely on the mass-to-charge ratio (m/q). This method not only facilitates mass measurements with a relative precision on the order of 10^{-6} within a brief measurement time of approximately 1 ms, covering nearly all relevant nuclear species, but also offers a more effective solution for compact storage rings compared to ion cooling by enabling efficient particle identification and velocity determination directly within the system [19]. In this way, the mass resolving power R of the isochronous ring spectrometer depends directly on the revolution time differences among the isotopes.

$$R = \frac{m}{\Delta m} = \frac{1}{\gamma_t^2}\frac{T}{\Delta T} .$$

Although an ideal isochronous ring theoretically cancels all momentum-dependent effects—both linear and higher-order—practical limitations such as imperfections and nonlinearities restrict this perfect cancellation to particles with momentum very close to that of the reference bunch. For particles with greater momentum deviations, chromaticity and resonance effects become significant, often requiring the application of corrective elements like sextupole magnets [20].

The present design of the ISRS ring utilizes a quadrupole gradient in each dipole magnet, following the FFAG configuration. This is highly effective in achieving high momentum acceptance, as the beam orbit is controlled within the ring by the gradient. Eventually, the ISRS ring is designed as a versatile system capable of operating under both isochronicity and quasi-isochronicity conditions for a broad range of ions.

3. Magnets

The optical configurations addressed in this work are based on the dimensions and field specifications of the MAGDEM prototype, developed for the ISRS project, a state-of-the-art Nb-Ti superconducting CCT magnet [21]. As one of the most advanced magnets of its kind to be manufactured, MAGDEM features a groundbreaking design that integrates dipole and quadrupole coils into a single, compact, tapered structure. This dual-functionality enhances field quality and operational efficiency while optimizing space utilization, addressing in this way the stringent demands of modern accelerator systems. A view of the mechanical design of the MAGDEM system, along with the coil geometry, is shown in Fig. 2.

The MAGDEM's specifications are summarized in Table 1. The magnet has a total length of 720 mm and an effective magnetic length of 580 mm, and is designed to bend beams by 36°. Field errors are minimized to below 1/10,000 along the tightly curved trajectory, even at peak magnetic fields approaching 4 T. To illustrate the combined dipole and quadrupole field distributions, a field map of the MAGDEM design is shown in Fig. 3. The use of tapered straight tubes simplifies assembly and allows for the application of radial pre-stress, which significantly enhances mechanical stability. Operating at approximately 100 A, the MAGDEM design minimizes heat leakage while maintaining a cryogenic temperature of 4.5 K with a single cryocooler, thereby ensuring high energy efficiency.

The nested CCT layers in MAGDEM are wound at opposing skew angles, enabling the simultaneous generation of dipole and quadrupole fields with exceptional field quality and minimal higher-order harmonics. This innovative configuration ensures precise control over radioactive ion beams, highly suitable for effectively guiding and bending them within the ISRS storage ring. MAGDEM represents an example of cutting-edge magnet technology, combining high performance with a compact design to meet the technological challenges in nuclear physics experiments and beyond.

For beam injection and extraction, the ISRS ring is expected to incorporate dedicated magnetic systems, including septum and kicker magnets. However, within the mechanical layout envisioned for MAGDEM, and given the very limited space available between consecutive bending magnets, the integration of an injection system capable of handling beams with high magnetic rigidity presents several challenges and is currently under investigation.

In our case, Superconducting Shield (SuShi) septum magnets [22] are being considered, as they can provide efficient beam deflection within highly compact geometries. Other alternatives based on compact, high-field septum magnets are also under evaluation [23]. Consequently, a joint development effort between the main ring magnet and the set of auxiliary magnets required to guide the beam along a strongly curved trajectory from the exterior into the ring becomes necessary. On the other hand, high-speed RF kickers are required to enable precise beam injection [24]. The preliminary design under consideration aims to initiate injection (and, symmetrically, extraction) through one or two of the ring magnets, taking advantage of the quadrupolar field component present in their design. This approach allows the correction angle required from the RF kicker to be significantly reduced, to below 50 mrad. Nevertheless, the trajectories followed by the injected beam remain constrained by the physical apertures of the magnets involved.

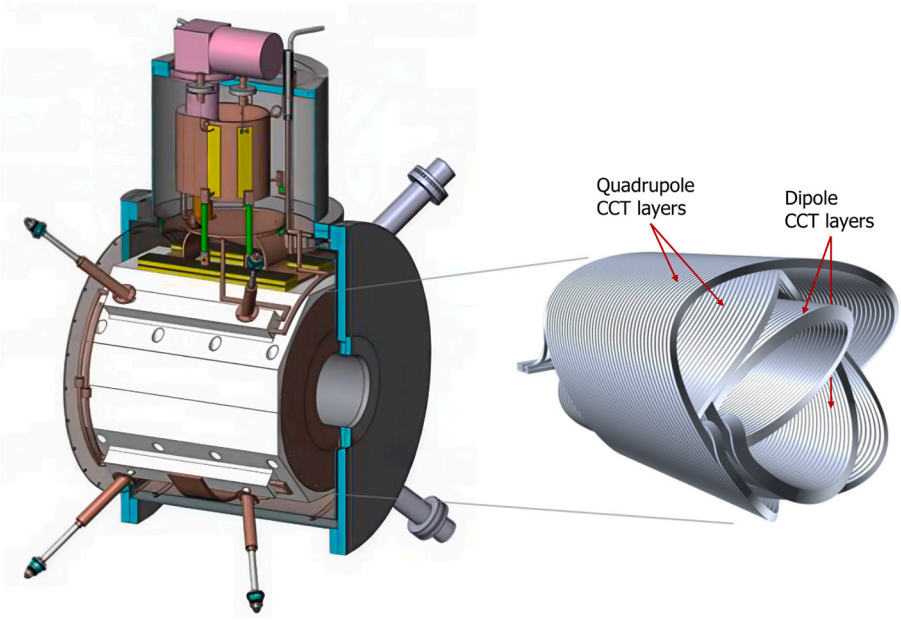

Fig. 2. View of the MAGDEM fully integrated system (left) and the CCT coils (right).

Table 1
Key specifications of the MAGDEM magnet [21].

Parameter	Value
Magnet type	Nested dipole and quadrupole CCT
Total length [mm]	720
Effective magnetic length [mm]	580
Bore aperture diameter [mm]	200
Mechanical diameter [mm]	900
Dipole field strength [T]	<2.3
Beam bending capacity [degrees]	36
Quadrupole field gradient [T/m]	<9.8
Operating current [A]	~ 100
Cryogenic temperature [K]	4.5
Field error [ppm]	<100

For this reason, both the magnetic and mechanical design of these elements must be appropriately adapted to meet the beam-dynamics requirements of injection and extraction systems beyond the currently developed MAGDEM technological demonstrator.

The beam dynamics analyses presented in this article are therefore limited to the tracking of ion beams already injected into the machine, as they provide valuable insight into the separation power of the spectrometer and its main acceptance limitations. Further development of the complete ring design through more realistic simulations will depend on the ongoing development of new demonstrators featuring magnetic systems capable of integrating beam injection and extraction.

4. Ion optics of the ISRS ring

The general layout of the ISRS ring is shown in Fig. 1. The lattice consists of two symmetric arcs, each comprising five MAGDEM-type CCT magnets arranged in an alternating FDFDF quadrupole pattern, where "F" and "D" denote horizontal focusing and defocusing modes, respectively. Additionally, two 1-m-long drift sections have been incorporated to ensure mechanical clearance between magnets and to accommodate critical subsystems. The first long drift section is reserved for injection and extraction components, including the RF kicker, while the opposite drift section hosts ToF detectors. This location benefits from the large horizontal off-momentum dispersion in the region, optimizing the accuracy of magnetic rigidity measurements while performing simultaneous ToF measurements [25].

Beam dynamics studies for the ISRS ring are conducted using the Xsuite code [26], which models the reference lattice using dipole and quadrupole elements. The combined dipole-quadrupole function magnets are implemented in this code as rectangular bending magnets (RBEND) incorporating a quadrupole-mode field gradient. The analysis is restricted to first-order calculations, focusing on the characterization of the ring tuning and resonances.

The lattice configurations for the isochronous and quasi-isochronous operation modes of the ring are structurally similar, with the key difference being the adjustments to the quadrupole gradients of the magnets. Following the same symmetry used in the ring layout for the beam lattice, the five magnets share identical quadrupole field configurations in both arcs. Additionally, each arc exhibits mirror symmetry with respect to the central magnet. Therefore, we denote the horizontal

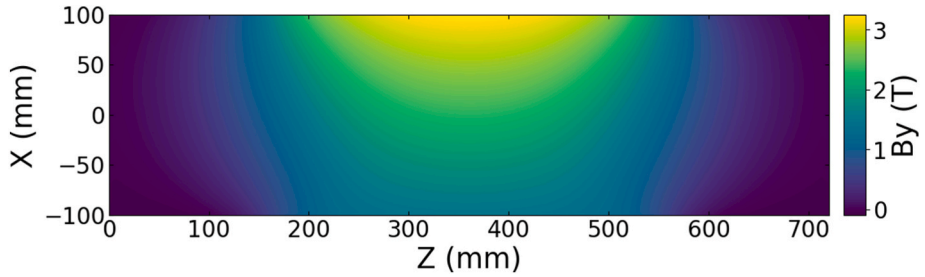

Fig. 3. Vertical component of the MAGDEM magnetic-field map, showing the combination of a 2.3 T dipole field and a quadrupole field with a gradient of 10 T/m.

focusing strength of the outer magnets as QF1, the defocusing strength of the inner magnets as QD, and the focusing strength of the central magnet as QF2 (see Fig. 1).

4.1. Isochronous mode

The core study of the ring focuses on achieving an isochronous mode, where the transition gamma (γ_t) aligns with the Lorentz gamma factor, $\gamma = 1.01054$ for $^{234}Ra^{+53}$ ions at 10 MeV/u. This condition is attained through precise adjustments of the quadrupole magnet gradients. The central magnet in each arc plays a key role, acting as the effective combined magnet to ensure the desired isochronicity. The nominal gradient values for both isochronous and quasi-isochronous conditions are presented in Table 2 and the designed optical functions for the isochronous optics are represented in Fig. 4. With these settings, the betatron tunes of the ring are adjusted to $(Q_x, Q_y) = (1.04, 1.27)$. A maximum first order horizontal dispersion of $D_x^{\max} \simeq 2.1$ m is achieved, with a focal point at the center of the long drift section, which would make it an ideal location for placing ToF detectors with enhanced spatial measurement resolution. This dispersion upper bound defines the range of off-momentum orbits that the ring can accommodate within the aperture limits of its elements, primarily the 200 mm bore aperture diameter of the magnets (d_{ap}), corresponding to a maximum momentum acceptance $\langle \Delta P/P \rangle_{MA} \simeq 4.76\%$, calculated from the maximum dispersion of the ring:

$$\langle \Delta P/P \rangle_{MA}[\%] = \frac{d_{ap}}{2D_x^{\max}} \cdot 100 \,. \tag{2}$$

The corresponding momentum acceptance contours based on Eq. (2) are shown in Fig. 5. However, it is important to note that these momentum acceptance estimates, based on the physical apertures of the elements, tend to overestimate the actual value. In the momentum acceptance analysis, optical resonance effects must also be taken into account as a limiting condition, as we will see in Section 5.

4.2. Quasi-isochronous mode

The second configuration of the ring, featuring a transition gamma of $\gamma_t = 1.16268$, is tailored to achieve a higher momentum acceptance. By reducing the maximum horizontal dispersion, this setup enables the inclusion of a broader momentum range of particles, thereby increasing overall beam intensity. However, this comes at the cost of mass-to-charge (m/q) separation, as the beam distribution becomes tilted in longitudinal phase space, that is, with a degree of correlation between time and momentum (or velocity). This correlation results from the significant mismatch between the transition gamma and the Lorentz gamma of the reference beam, $\gamma = 1.01054$, compromising isochronicity.

Table 2
Beam dynamics properties of the reference $234Ra^{+53}$ beam, and dipole field and quadrupole normalized gradients of operation of the magnets for the isochronous and quasi-isochronous modes.

	Isochronous	Quasi-isochronous
Ring path length [m]	11.54	11.54
Beam energy [MeV/u]	10	10
Magnetic rigidity, $B\rho$ [T·m]	2	2
Beam Lorentz factor, γ	1.01054	1.01054
Transition factor, γ_t	1.01054	1.16268
Max Dispersion, $D_x^{\max}$ [cm/%]	2.1	1.9
Betatron tune, Q_x	1.04	1.15
Betatron tune, Q_y	1.27	1.21
Dipole field [T]	2.1266	
Quadrupole field, QF1 [T/m]	2.273	2.331
Quadrupole field, QD [T/m]	−2.007	−1.932
Quadrupole field, QF2 [T/m]	3.691	4.740

Fig. 4 illustrates the betatron functions and dispersion curve for this lattice. The maximum horizontal dispersion reaches $D_x^{\max} \simeq 2.0$, which is slightly lower than in the isochronous mode. In this case, considering Eq. (2), the maximum momentum acceptance is approximately 5%. The betatron amplitudes remain close to their minimum values, ensuring beam stability. Furthermore, the higher β-function at the injection point significantly boosts the acceptance of injected particles, thereby improving overall beam performance.

Sharing the same layout as the isochronous setup and just adjusting the quadrupole gradients at the MAGDEM-type magnets, this configuration achieves not only a larger momentum acceptance but, as we will see in the following section, also offers a more robust stability by shifting the betatron tunes away from resonances.

5. Betatron tunes and resonances

Particles with varied momenta within the reference bunch traverse different trajectories in the ring. This phenomenon results in the changes of the tuning conditions for the main bunch m/q due to the chromatic effects introduced by the magnetic elements in the beamline. The resolution power of the spectrometer is influenced by these chromatic effects.

Fig. 6 illustrates the deviation of the vertical and horizontal tunes due to momentum differences. From these data, the chromaticity ξ of the ring is calculated, representing the variation in the betatron tune as a function of the momentum change, expressed as:

$$\xi_{x,y} = \frac{\mathrm{d}Q_{x,y}}{\mathrm{d}(\Delta P/P)} \,.$$

This calculation is performed for relative momentum deviations ranging from −5 to 5%, as the orbit is not closed for larger deviations in the isochronous mode. The calculated chromaticity (horizontal and vertical) around the reference momentum for the isochronous and quasi-isochronous configurations are $(\xi_x, \xi_y) = (3.826, -0.351)$ and $(\xi_x, \xi_y) = (3.213, -0.435)$, respectively.

Chromaticity can broaden the energy spread and make the beam distorted, thus hindering isochronous operation for particles with momentum deviation different from that of the reference beam. A sufficiently small chromaticity helps maintain tune stability associated with the isochronous condition over a large number of revolutions within a specific energy range, preferably within 1σ of the momentum spread. In the case of non-isochronous rings, this chromaticity becomes significantly large even with linear lattice elements, leading to alterations in particle trajectories and timing. The discontinuities in Fig. 6 indicate critical resonance line crossing. This can be observed more clearly in the tune diagram in Fig. 7, where we show the working points of the two proposed configurations along with resonance lines up to the fourth order. The resonance condition is determined by:

$$aQ_x + bQ_y = c,$$

with a, b, and c being arbitrary integers, and $|a| + |b|$ gives the order of the resonance.

The position of the reference beams relative to the resonances determines the beam's stability range in momentum against magnetic imperfections in the ring's lattice elements. This is the case for the isochronous mode, where particles with a momentum deviation of −1% produce betatron tunes at the edge of a first-order resonance line, which limits its operational capability. In contrast, the quasi-isochronous operating mode benefits from a working point farther away from low-order resonance lines, ensuring greater stability over a wider energy range. The first-order resonance is encountered at a momentum deviation close to −3%.

The momentum acceptance of the ring is therefore constrained by stability criteria associated with the tune resonances. As shown in Fig. 7, the momentum acceptance is approximately 1%, which is about five

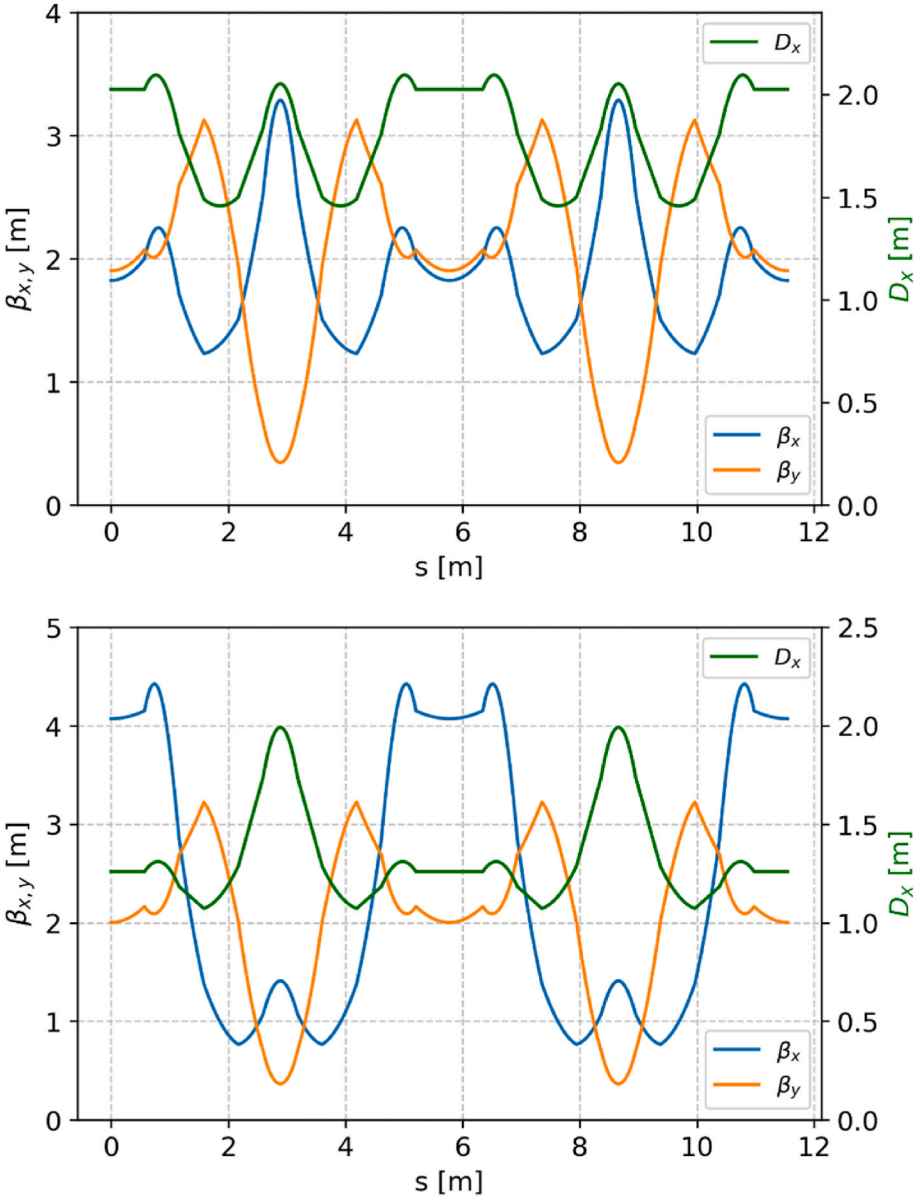

Fig. 4. Betatron functions $\beta_{xy}(s)$ and first order dispersion $D_x(s)$ for the ISRS isochronous (top) and quasi-isochronous (bottom) optical operation modes.

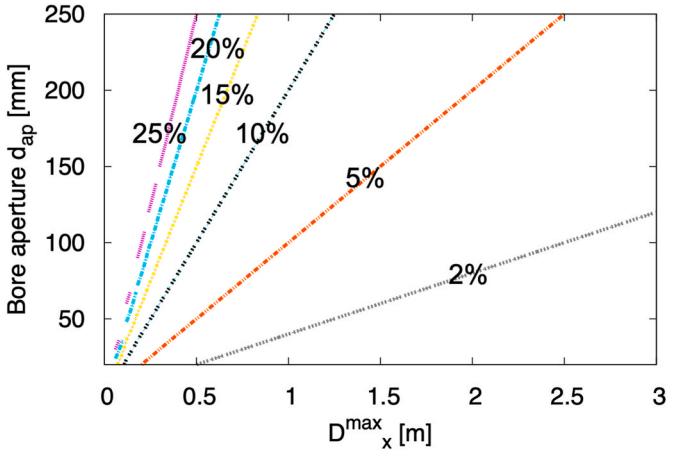

Fig. 5. Momentum acceptance contours as a function of the physical aperture of the lattice elements and the maximum horizontal dispersion within the ring.

times lower than the value obtained by considering only the dispersion and the geometric bore aperture using Eq. (2).

To mitigate chromatic effects and maintain stable beam tuning across momentum deviations, corrections with nonlinear magnetic elements, such as sextupoles, are required. However, the ability of quasi-isochronous rings to accommodate higher-momentum particles without the need for additional corrector elements, underscores their advantage in applications requiring broader momentum acceptance.

6. Time-of-Flight calculations

ToF techniques are essential tools for the separation and identification of particles based on their mass and charge. This principle underlies the operation of isochronous spectrometers such as the ISRS. Unlike conventional linear spectrometers, where time resolution is strongly dependent on the total system length, an isochronous ring can achieve effective mass and charge ion separation after only a few revolutions of the beam, enabling a more compact setup without compromising precision.

Detectors are adaptable to experimental requirements, being either

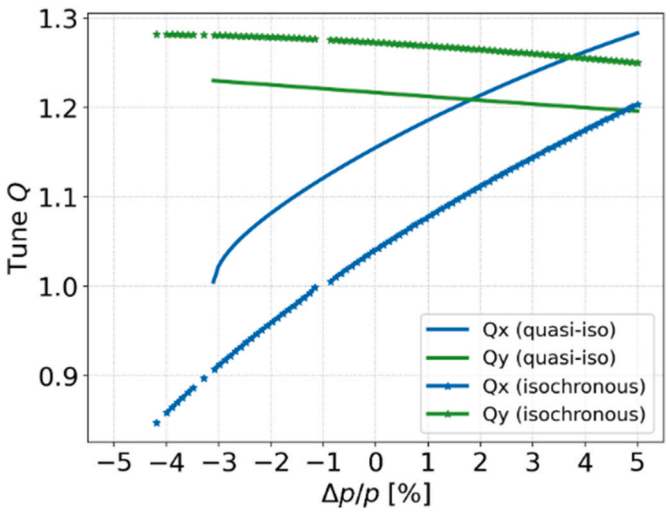

Fig. 6. Horizontal and vertical betatron tune dependence on the momentum deviation with respect to reference beam, for both isochronous and quasi-isochronous configurations.

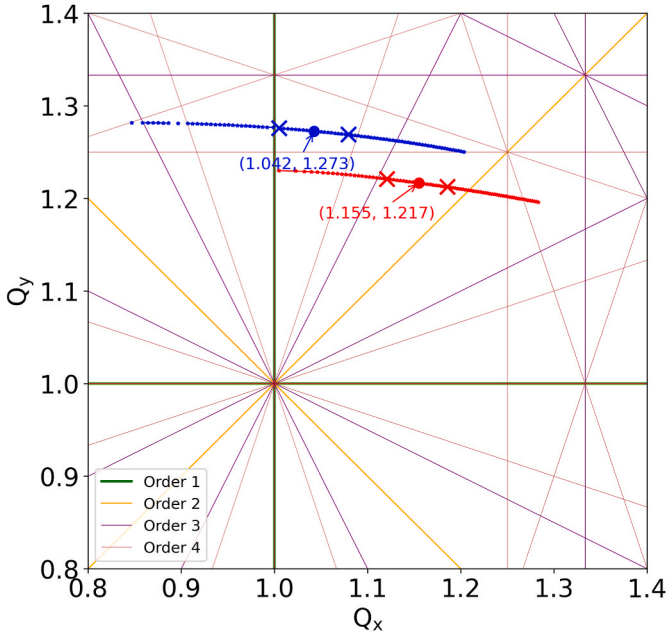

Fig. 7. Tune working points on the tune-resonance diagram for different momentum deviations, ranging from −5 to +5%, for the reference beam of isochronous and quasi-isochronous configurations. Circular markers indicate the tune working points for the reference ion, while cross markers correspond to momentum deviations of −1% and +1%.

integrated inside the ring or positioned externally after particle extraction. The application of this system is further refined through the Xsuite code framework, which provides particle tracking calculations over time and manages bunches with diverse mass and charge ratios. This framework ensures precise simulations and optimization of experimental setups involving quasi-isochronous or isochronous systems.

An example involving nine bunches of Ra isotopes with different masses (233-235) and charges (+52 to +54) is presented. Simulations have been performed using a set of 5000 macroparticles for each bunch type, and the ToF separation has been evaluated for both the isochronous and quasi-isochronous configurations of the same ring. The bunches are initialized at the midpoint between the two symmetric arcs, where the injection kicker is expected to be located. The corresponding beam parameters are summarized in Table 3. All bunches are initialized with identical beta and dispersion values, matched to the ring optics for each configuration, and the Twiss $\alpha_{x,y}$ parameter is set to zero to ensure a balanced phase-space distribution. The assumed transverse emittance of 12.5 mm mrad reflects a realistic phase-space profile for nuclear reaction products in an ISOLDE-type experiment. All bunches also share the same distribution in longitudinal phase space, with an average kinetic energy of 10 MeV per nucleon. Time and relative momentum deviation have been varied according to a Gaussian distribution with RMS spreads of 1 ns and 1%, respectively.

The bending and focusing strengths of the ring magnets are tuned so that the reference ion, $^{234}Ra^{+53}$, follows the reference orbit. The other ions traverse their trajectories in the different orbits depending on their specific mass and charge, due to the differences in magnetic rigidity.

In isochronous mode, the reference ion describes an 11.542-m orbit in 267.5 ns per revolution, completing 10 revolutions in a total time of 2675 ns. Analysis of the arrival times, shown in Fig. 8, reveals that ions with a higher charge state (+54) arrived earlier than those with the reference charge state (+53). Among the isotopes that have been studied, $^{233}Ra^{+53}$, with a lower mass, arrived 11.5 ns earlier than the reference ion, while $^{235}Ra^{+53}$, with a higher mass, arrived 11 ns later.

For particles with momentum deviations beyond ±1%, bunches exhibited slight nonlinear effects, leading to short tails in the histogram plot. Particles with magnetic rigidities significantly different from that of the reference beam suffered greater losses, up to 30% for $^{234}Ra^{+54}$, due to the aperture limitations of the CCT magnets. These particles also exhibited stronger nonlinearities, resulting in a broader full-width at half-maximum (FWHM) in the detector signal, ultimately degrading the resolution.

Nonetheless, due to the isochronous nature of the ring, the bunches effectively preserve a much narrower temporal structure than the observed separations. This highlights the ring's strong mass-separation capability, even for very heavy ion species with extremely small mass differences.

In the quasi-isochronous ring, particles with bigger momentum were effectively accepted, shown in Fig. 9, with losses remaining below 10% for $^{234}Ra^{+54}$. No significant nonlinear effects were observed in the bunches. Since the beam mean energy and velocity is away from the transition gamma, the bunches experienced longitudinal spread, thus leading to a reduction in time-resolving power. Under these conditions, the time separation between bunches with the same charge state was approximately 8.5 ns, still sufficient to separate and identify the species in the ToF diagnostic signal. Despite the loss in temporal resolution, detection systems at a given focal plane would combine the ToF signals with beam kinetic energy measurements, enabling a more precise separation of different isotopes within this diagnostic map, as shown in Fig. 10.

7. Conclusions

The development of the ISRS ring represents a significant advancement in the separation of short-lived radionuclides. Its highly compact design, fitting within a 5×5 m^2 footprint, and the integration of specialized, strong-bending, large-aperture CCT magnets demonstrate

Table 3
Initial beam parameters at the kicker location used for tracking simulations of time-of-flight separation.

Parameter	Isochronous	Quasi-isochronous
Horizontal beta function, β_x [m]	1.79	4.10
Vertical beta function, β_y [m]	1.90	2.01
Horizontal dispersion, D_x [cm/%]	2.03	1.26
Horizontal emittance, ϵ_x [mm·mrad]	12.5	12.5
Vertical emittance, ϵ_y [mm·mrad]	12.5	12.5
Relative momentum spread, $\sigma_{\Delta P/P}$ [%]	1	1
Bunch length in time, σ_t [ns]	1	1

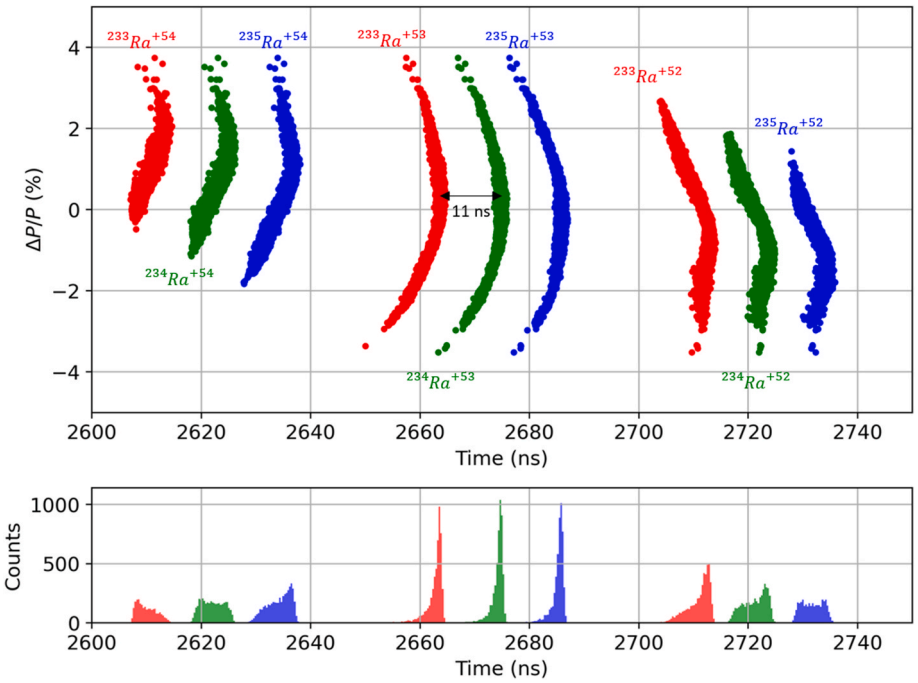

Fig. 8. Time and relative momentum deviation distribution with respect to the reference ion $^{234}Ra^{+53}$ (top) for the simulated species in the isochronous configuration of the ISRS ring after ten revolutions. Projected time-of-flight signals for each species (bottom).

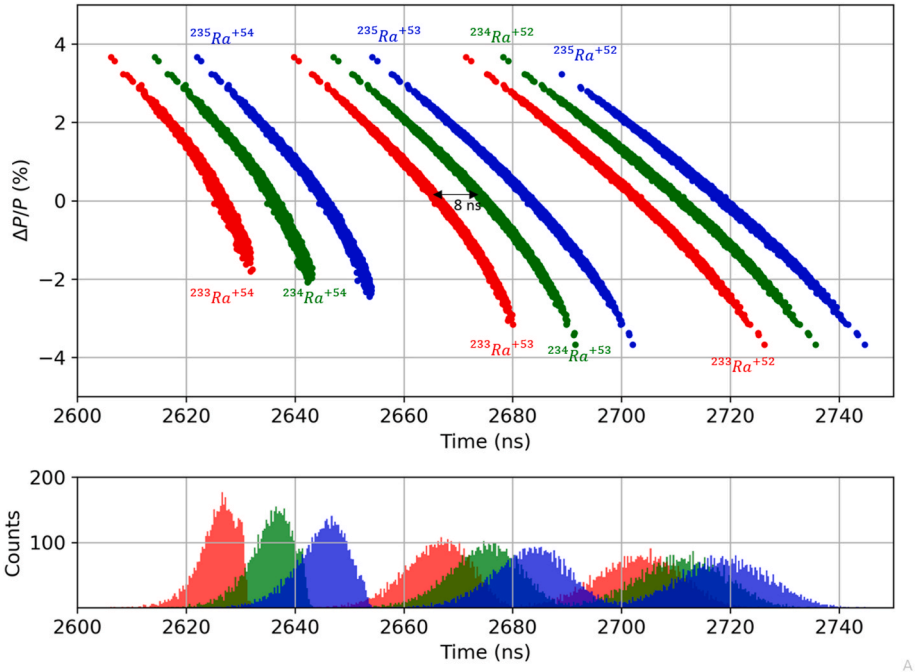

Fig. 9. Time and relative momentum deviation distribution with respect to the reference ion $^{234}Ra^{+53}$ (top) for the simulated species in the quasi-isochronous configuration of the ISRS ring after ten revolutions. Projected time-of-flight signals for each species (bottom).

excellent performance, comparable to that of other separation rings. A key strength of the system is its ability to efficiently handle particles with high magnetic rigidity.

Although chromaticity effects in isochronous mode present certain challenges, the FFAG-inspired design of the ring enables quasi-isochronous operation, effectively mitigating these issues. In isochronous mode, the bunches preserve their temporal structure on the nanosecond scale, thereby achieving outstanding charge-to-mass separation. For very short storage times, as few as 10 revolutions, the resulting ToF resolution corresponds to a charge-to-mass resolving power better than 1/2,600, significantly superior to that attainable with conventional linear spectrometers. By further increasing the beam storage time in the ring to the scale of several hundred microseconds, the spectrometer's resolving power could be greatly enhanced, thereby extending its capability to distinguish isomeric states of interest with decay times longer than the storage duration. Beam dynamics limitations for a large number of turns in the ring, such as the effects of dynamic aperture and slight deviations from isochronicity, will be studied

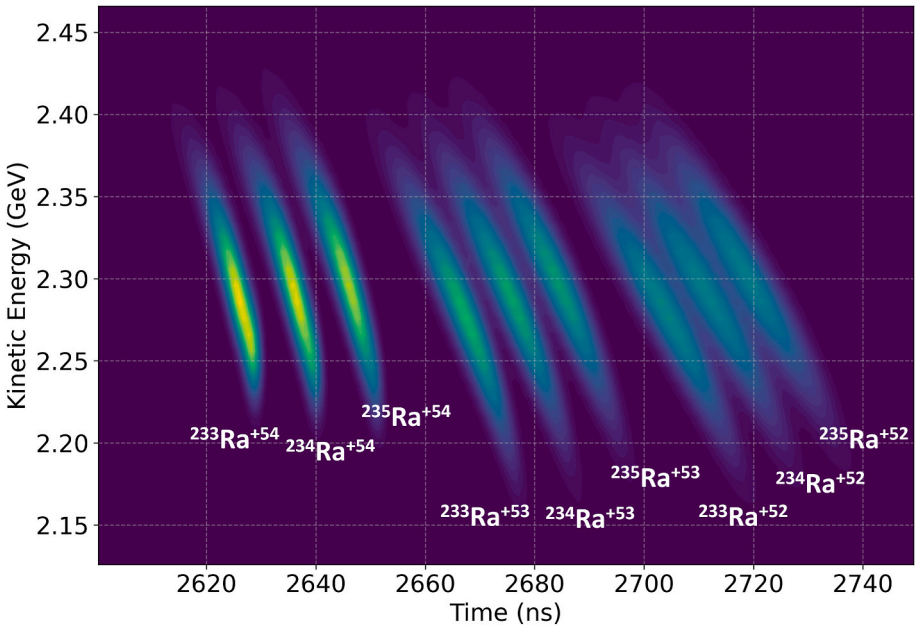

Fig. 10. Simulation of time and kinetic energy distribution at a focal plane inside the ring for Ra species in the quasi-isochronous configuration of the ISRS ring after ten revolutions.

in detail to enable potential nuclear physics experiments requiring ultra-high mass resolution.

Quasi-isochronous operation enhances momentum acceptance and provides greater stability against magnetic imperfections by shifting the tune working point away from resonance lines, allowing the ring to accommodate momentum spreads of up to ±1% without sextupole correction. This dual-mode capability extends the ring's applicability to higher-rigidity beams while maintaining overall beam stability.

Through precise beam dynamic calculations, the ISRS demonstrates effective isotope separation, particularly for very heavy ion beams, such as $^{234}Ra^{+53}$. The separation precision is well displayed in isochronous mode with 11 ns, and quasi-isochronous mode with 8 ns, after 10 revolutions. With a maximum energy of 10 MeV per nucleon, as achieved at HIE-ISOLDE, the ring is ideally suited for integration into this facility.

As part of the ISRS collaboration within the ISOLDE program, magnetic field measurements on the MAGDEM prototype currently under development will provide valuable input for the fine-tuning of the ring lattice. Future work will focus on incorporating realistic field maps into beam dynamics calculations and evaluating higher-order chromatic and nonlinear effects, with the aim of implementing corrections using sextupole magnets. In parallel, efforts are underway to fully implement the beam injection and extraction systems, which present a significant challenge for high-rigidity beams in such an extremely compact design. This will likely require the integration of high-field septum subsystems embedded within the main ring magnets.

The ISRS ring's ability to operate in both isochronous and quasi-isochronous modes makes it a versatile and powerful tool for the study of nuclear astrophysics and exotic isotopes. This enables high-resolution ToF measurements and broad momentum acceptance, providing critical insights into rare and short-lived nuclear species.

CRediT authorship contribution statement

Fazel Taft: Writing – original draft, Visualization, Validation, Software, Resources, Methodology, Investigation, Data curation. **Jorge Giner Navarro:** Writing – review & editing, Validation, Supervision, Methodology. **Teresa Kurtukian-Nieto:** Writing – review & editing, Validation, Funding acquisition, Conceptualization. **Ismael Martel:** Writing – review & editing, Validation, Funding acquisition, Conceptualization. **Javier Resta-López:** Writing – review & editing, Visualization, Validation, Supervision, Funding acquisition, Conceptualization.

Declaration of competing interest

The authors declare that they have no known competing financial interests or personal relationships that could have appeared to influence the work reported in this paper.

Acknowledgements

This work has been financially supported by the Spanish Government under the grant agreement “Experiment ISRS-ISOLDE” (BOE-A-2023-16885), the “Recovery, Transformation and Resilience Plan”, the European Union program “Next Generation EU”, and the Spanish Ministry of Science and Innovation under grant agreements PID2021-127711NB-I00, PID2024-159209NB-C21 and PID2024-159209NB-C22.

References

[1] K. Blaum, J. Dilling, W. Nörtershäuser, Precision atomic physics techniques for nuclear physics with radioactive beams, Phys. Scripta 2013 (2013) 014017, https://doi.org/10.1088/0031-8949/2013/T152/014017.

[2] B. Franzke, H. Geissel, G. Münzenberg, Mass and lifetime measurements of exotic nuclei in storage rings, Mass Spectrom. Rev. 27 (2008) 428–469, https://doi.org/10.1002/mas.20173.

[3] Y. Abe, Y. Yamaguchi, M. Wakasugi, H. Baba, T. Fujinawa, Z. Ge, A. Goto, S. Michimasa, H. Miura, T. Moriguchi, D. Nagae, S. Naimi, J. Ohnishi, S. Omika, S. Ota, A. Ozawa, F. Suzaki, H. Suzuki, S. Suzuki, N. Tadano, A. Tokuchi, T. Uesaka, K. Wakayama, T. Yamaguchi, Y. Yano, Performance of a precise isochronous magnetic field over a wide momentum range in the Rare-RI ring, Nucl. Instrum. Methods Phys. Res. Sect. Accel. Spectrometers Detect. Assoc. Equip. 1072 (2025) 170083, https://doi.org/10.1016/j.nima.2024.170083.

[4] K. Blaum, High-accuracy mass spectrometry with stored ions, Phys. Rep. 425 (2006) 1–78, https://doi.org/10.1016/j.physrep.2005.10.011.

[5] T. Radon, H. Geissel, G. Münzenberg, B. Franzke, Th Kerscher, F. Nolden, YuN. Novikov, Z. Patyk, C. Scheidenberger, F. Attallah, K. Beckert, T. Beha, F. Bosch, H. Eickhoff, M. Falch, Y. Fujita, M. Hausmann, F. Herfurth, H. Irnich, H. C. Jung, O. Klepper, C. Kozhuharov, YuA. Litvinov, K.E.G. Löbner, F. Nickel, H. Reich, W. Schwab, B. Schlitt, M. Steck, K. Sümmerer, T. Winkler, H. Wollnik, Schottky mass measurements of stored and cooled neutron-deficient projectile fragments in the element range of 57≤Z≤84, Nucl. Phys. 677 (2000) 75–99, https://doi.org/10.1016/S0375-9474(00)00304-3.

[6] M. Steck, Y.A. Litvinov, Heavy-ion storage rings and their use in precision experiments with highly charged ions, Prog. Part. Nucl. Phys. 115 (2020) 103811, https://doi.org/10.1016/j.ppnp.2020.103811.
[7] M. Zhang, X. Zhou, M. Wang, Y.H. Zhang, YuA. Litvinov, H.S. Xu, R.J. Chen, H. Y. Deng, C.Y. Fu, W.W. Ge, H.F. Li, T. Liao, S.A. Litvinov, P. Shuai, J.Y. Shi, R. S. Sidhu, Y.N. Song, M.Z. Sun, S. Suzuki, Q. Wang, Y.M. Xing, X. Xu, T. Yamaguchi, X.L. Yan, J.C. Yang, Y.J. Yuan, Q. Zeng, X.H. Zhou, $B\rho$-defined isochronous mass spectrometry and mass measurements of ^{58}Ni fragments, Eur. Phys. J. A 59 (2023) 27, https://doi.org/10.1140/epja/s10050-023-00928-6.
[8] I. Martel, L. Acosta, J.L. Aguado, M. Assie, M.A.M. Al-Aqeel, A. Ballarino, D. Barna, R. Berjillos, M. Bonora, C. Bontoiu, M.J.G. Borge, J.A. Briz, I. Bustinduy, L. Bottura, L. Catalina-Medina, W. Catford, J. Cederkäll, T. Davinson, G. de Angelis, A. Devred, C. Díaz-Martín, T. Ekelöf, H. Felice, H. Fynbo, A.P. Foussat, R. Florin, S.J. Freeman, L. Gaffney, C. García-Ramos, L. Gentini, C.A. Gonzalez-Cordero, C. Guazzoni, A. Haziot, A. Heinz, J.M. Jimenez, K. Johnston, B. Jonson, G. Kirby, O. Kirby, T. Kurtukian-Nieto, M. Labiche, M. Liebsch, M. Losasso, A. Laird, J.L. Muñoz, B. S. Nara Singh, G. Neyens, P.J. Napiorkowski, D. O'Donnell, R.D. Page, D. Perini, J. Resta-López, G. Riddone, J.A. Rodriguez, V. Rodin, S. Russenschuck, V. R. Sharma, F. Salguero-Andújar, J. Sánchez-Segovia, K. Riisager, A.M. Sánchez-Benítez, B. Shepherd, E. Siesling, J. Smallcombe, M. Stanoiu, O. Tengblad, J. P. Thermeau, D. Tommasini, J. Uusitalo, S. Varnasseri, C.P. Welsch, G. Willering, An innovative superconducting recoil separator for HIE-ISOLDE, Nucl. Instrum. Methods Phys. Res. Sect. B Beam Interact. Mater. At. 541 (2023) 176–179, https://doi.org/10.1016/j.nimb.2023.05.052.
[9] Y. Kadi, M.A. Fraser, A. Papageorgiou-Koufidou, Y. Kadi, HIE-ISOLDE: Technical Design Report for the Energy Upgrade, CERN, Geneva, 2018, https://doi.org/10.23731/CYRM-2018-001.
[10] C. Bontoiu, I. Martel, J. Resta-López, V. Rodin, C.P. Welsch, Conceptual design of a novel and compact superconducting recoil separator for radioactive isotopes, Nucl. Instrum. Methods Phys. Res. Sect. Accel. Spectrometers Detect. Assoc. Equip. 969 (2020) 164048, https://doi.org/10.1016/j.nima.2020.164048.
[11] P. Reiter, N. Warr, Nuclear structure studies with re-accelerated beams at REX-and HIE-ISOLDE, Prog. Part. Nucl. Phys. 113 (2020) 103767, https://doi.org/10.1016/j.ppnp.2020.103767.
[12] J. Resta-López, A. Foussat, G. Kirby, I. Martel, V. Rodin, Design and Beam Dynamics Studies of a Novel Compact Recoil Separator Ring for Nuclear Research with Radioactive Beams, JACOW Publishing, Geneva, Switzerland, 2021, pp. 3031–3034, https://doi.org/10.18429/JACoW-IPAC2021-WEPAB180.
[13] D. Trbojevic, E. Keil, A. Sessler, Non-Scaling Fixed Field Gradient Accelerator (FFAG) Design for the Proton and Carbon Therapy, BROOKHAVEN NATIONAL LABORATORY, 2005. https://www.osti.gov/biblio/15020025. (Accessed 3 December 2025).
[14] S. Machida, Fixed field alternating gradient. https://doi.org/10.5170/CERN-2013-001.33, 2013.
[15] M. Hausmann, F. Attallah, K. Beckert, F. Bosch, A. Dolinskiy, H. Eickhoff, M. Falch, B. Franczak, B. Franzke, H. Geissel, T. Kerscher, O. Klepper, H.-J. Kluge, C. Kozhuharov, K.E.G. Löbner, G. Münzenberg, F. Nolden, YuN. Novikov, T. Radon, H. Schatz, C. Scheidenberger, J. Stadlmann, M. Steck, T. Winkler, H. Wollnik, First isochronous mass spectrometry at the experimental storage ring ESR, Nucl. Instrum. Methods Phys. Res. Sect. Accel. Spectrometers Detect. Assoc. Equip. 446 (2000) 569–580, https://doi.org/10.1016/S0168-9002(99)01192-4.
[16] YuA. Litvinov, H. Geissel, T. Radon, F. Attallah, G. Audi, K. Beckert, F. Bosch, M. Falch, B. Franzke, M. Hausmann, M. Hellström, Th Kerscher, O. Klepper, H.-J. Kluge, C. Kozhuharov, K.E.G. Löbner, G. Münzenberg, F. Nolden, YuN. Novikov, W. Quint, Z. Patyk, H. Reich, C. Scheidenberger, B. Schlitt, M. Steck, K. Sümmerer, L. Vermeeren, M. Winkler, Th Winkler, H. Wollnik, Mass measurement of cooled neutron-deficient bismuth projectile fragments with time-resolved Schottky mass spectrometry at the FRS-ESR facility, Nucl. Phys. 756 (2005) 3–38, https://doi.org/10.1016/j.nuclphysa.2005.03.015.
[17] Y.A. Litvinov, H. Geissel, R. Knöbel, B. Sun, H. Xu, Direct mass measurements of exotic nuclei in storage rings, Acta Phys. Pol. B 41 (2010) 511–523.
[18] S.A. Litvinov, Investigation of the Isochronous Mode of the Experimental Storage Ring (ESR) and the Collector Ring (CR). Decay Spectroscopy of Highly Charged Stored ^{140}Pr Ions at the FRS-ESR Facility, GSI, 2008. https://repository.gsi.de/record/55262/export/print?ln=en. (Accessed 3 December 2025).
[19] D. Nagae, S. Omika, Y. Abe, Y. Yamaguchi, F. Suzaki, K. Wakayama, N. Tadano, R. Igosawa, K. Inomata, H. Arakawa, K. Nishimuro, T. Fujii, T. Mitsui, T. Yamaguchi, T. Suzuki, S. Suzuki, T. Moriguchi, M. Amano, D. Kamioka, A. Ozawa, S. Naimi, Z. Ge, Y. Yanagisawa, H. Baba, S. Michimasa, S. Ota, G. Lorusso, YuA. Litvinov, M. Wakasugi, T. Uesaka, Y. Yano, Isochronous mass spectrometry at the RIKEN Rare-RI ring facility, Phys. Rev. C 110 (2024) 014310, https://doi.org/10.1103/PhysRevC.110.014310.
[20] S. Litvinov, D. Toprek, H. Weick, A. Dolinskii, Isochronicity correction in the CR storage ring, Nucl. Instrum. Methods Phys. Res. Sect. Accel. Spectrometers Detect. Assoc. Equip. 724 (2013) 20–26, https://doi.org/10.1016/j.nima.2013.05.057.
[21] G. Kirby, N. Deelen, A. Iziquel, J. Van Nugteren, E. Page-Mason, D. Martins, R. Berjillos, C.G. Ramos, C.A.G. Cordero, T. Junquera, T. Kurtukian-Nieto, J. Resta, I. Martel, Design and optimization of a 4 tesla 200 mm aperture helium-free Nb-Ti nested CCT quadrupole/dipole superconducting magnet, IEEE Trans. Appl. Supercond. (2025) 1–7, https://doi.org/10.1109/TASC.2025.3529629.
[22] D. Barna, J. Borburgh, M. Atanasov, G. Kirby, G. Giunchi, V. Kárpáti, M. Szűcs, G. Szabó, V. Mertinger, The superconducting shield (SuShi) septum magnet prototype, IEEE Trans. Appl. Supercond. 32 (2022) 1–5, https://doi.org/10.1109/TASC.2022.3149726.
[23] K. Sugita, Novel concept of truncated iron-yoked cosine theta magnets and design studies for FAIR septum magnets, IEEE Trans. Appl. Supercond. 22 (2012), https://doi.org/10.1109/TASC.2011.2174953, 4902204–4902204.
[24] M.J. Barnes, L. Ducimetiere, T. Fowler, V. Senaj, L. Sermeus, Injection and extraction magnets: kicker magnets. https://doi.org/10.5170/CERN-2010-004.141, 2010.
[25] H. Geissel, D.J. Morrissey, Exotic nuclei and their separation, electromagnetic devices, in: Handb. Nucl. Phys., Springer, Singapore, 2023, pp. 3–61, https://doi.org/10.1007/978-981-19-6345-2_100.
[26] G. Iadarola, A. Abramov, P. Belanger, X. Buffat, R. De Maria, D. Demetriadou, L. Deniau, D. Di Croce, P. Hermes, P. Kicsiny, P. Kruyt, A. Latina, S. Łopaciuk, L. Mether, P. Niedermayer, K. Paraschou, T. Pieloni, M. Seidel, G. Sterbini, F. Van der Veken, L. van Riesen-Haupt, Xsuite: an integrated beam physics simulation framework, in: JACOW Publishing, 2024, pp. 73–80, https://doi.org/10.18429/JACoW-HB2023-TUA2I1. Geneva, Switzerland.